Author Manuscript

Author Manuscript

Author Manuscript

Author Manuscript

HHS Public Access

Author manuscript

IEEE Trans Biomed Eng. Author manuscript; available in PMC 2023 February 01.

Published in final edited form as:

IEEE Trans Biomed Eng. 2022 February ; 69(2): 849–859. doi:10.1109/TBME.2021.3108135.

Robust Estimation of Respiratory Variability Uncovers Correlates of Limbic Brain Activity and Transcutaneous Cervical Vagus Nerve Stimulation in the Context of Traumatic Stress

Asim H. Gazi [Student Member, IEEE],
School of Electrical and Computer Engineering, S. Sundararaj is with the College of Sciences, Atlanta, GA 30308 USA

Matthew T. Wittbrodt,
Department of Anesthesiology, School of Medicine, Northwestern University, Chicago, IL 60611

Department of Psychiatry and Behavioral Sciences, Emory University School of Medicine, Atlanta, GA 30322

Anna B. Harrison [Student Member, IEEE],
School of Electrical and Computer Engineering, S. Sundararaj is with the College of Sciences, Atlanta, GA 30308 USA

Srirakshaa Sundararaj,
College of Sciences, Georgia Institute of Technology, Atlanta, GA 30308 USA

Nil Z. Gurel [Student Member, IEEE],
David Geffen School of Medicine at UCLA, Los Angeles, CA 90095

Jonathon A. Nye,
Department of Radiology, Emory University School of Medicine, Atlanta, GA 30322

Amit J. Shah,
Department of Epidemiology, Rollins School of Public Health, Atlanta, GA 30322

Department of Internal Medicine, Division of Cardiology, Emory University School of Medicine, Atlanta, GA 30322

Atlanta VA Medical Center, Emory University, Atlanta, GA 30322

Viola Vaccarino,
Department of Epidemiology, Rollins School of Public Health, Atlanta, GA 30322

Department of Internal Medicine, Division of Cardiology, Emory University School of Medicine, Atlanta, GA 30322

J. Douglas Bremner,
Department of Radiology, Emory University School of Medicine, Atlanta, GA 30322

corresponding author: asim.gazi@gatech.edu.

Color versions of one or more of the figures in this paper are available online at http://ieeexplore.ieee.org. This paper has supplementary downloadable multimedia material available at http://ieeexplore.ieee.org provided by the authors.

Author Manuscript Author Manuscript Author Manuscript Author Manuscript

Department of Psychiatry and Behavioral Sciences, Emory University School of Medicine, Atlanta, GA 30322

Atlanta VA Medical Center, Emory University, Atlanta, GA 30322

Omer T. Inan [Senior Member, IEEE]
School of Electrical and Computer Engineering, S. Sundararaj is with the College of Sciences

Coulter Department of Biomedical Engineering, Georgia Institute of Technology, Atlanta, GA 30308 USA

Abstract

Objective: Variations in respiration patterns are a characteristic response to distress due to underlying neurorespiratory couplings. Yet, no work to date has quantified respiration pattern variability (RPV) in the context of traumatic stress and studied its functional neural correlates – this analysis aims to address this gap.

Methods: Fifty human subjects with prior traumatic experiences (24 with posttraumatic stress disorder (PTSD)) completed a ~3-hr protocol involving personalized traumatic scripts and active/sham (double-blind) transcutaneous cervical vagus nerve stimulation (tcVNS). High-resolution positron emission tomography functional neuroimages, electrocardiogram (ECG), and respiratory effort (RSP) data were collected during the protocol. Supplementing the RSP signal with ECG-derived respiration for quality assessment and timing extraction, RPV metrics were quantified and analyzed. Specifically, correlation analyses were performed using neuroactivity in selected limbic regions, and responses to active and sham tcVNS were compared.

Results: The single-lag unscaled autocorrelation of respiration rate correlated negatively with left amygdala activity and positively with right rostromedial prefrontal cortex (rmPFC) activity for non-PTSD; it also correlated negatively with left and right insulae activity and positively with right rmPFC activity for PTSD. The single-lag unscaled autocorrelation of expiration time was greater following active stimulation for non-PTSD.

Conclusion: Quantifying RPV is of demonstrable importance to assessing trauma-induced changes in neural function and tcVNS effects on respiratory physiology.

Significance: This is the first demonstration of RPV's pertinence to traumatic stress- and tcVNS-induced neurorespiratory responses. The open-source processing pipeline elucidated herein uniquely includes both RSP and ECG-derived respiration signals for quality assessment, timing estimation, and RPV extraction.

Keywords

neural correlates; respiration signal processing; respiratory variability; stress; vagus nerve stimulation

I. Introduction

Distress generally involves engagement and withdrawal of the sympathetic ("fight or flight") and parasympathetic ("rest and digest") branches of the autonomic nervous system

Author Manuscript Author Manuscript Author Manuscript Author Manuscript

(ANS), respectively. A multitude of effects thereby manifest throughout the body, including respiratory variations that often result in a characteristic response: rapid and irregular breathing, breathlessness, and in some individuals, more severe responses such as panic attacks [1]. Although these effects are observed peripherally, internal communications between the central and peripheral nervous systems initiate and modulate these responses.

The respiratory center, located in the brainstem and distributed across the medulla and pons, acts as the primary mediator of these variations [2]. The center's positioning strategically facilitates integration of top-down signaling from subcortical and cortical regions of the brain (e.g., limbic system), and afferent signaling via the ANS (e.g., along the vagus nerve). The respiratory center's three respiratory groups – dorsal, ventral, and pontine – then signal efferently to the respiratory muscles to phase inspiration and expiration [3]. Notably, internal rhythm in the pre-Botzinger complex is not the only factor driving inspiration and expiration; rather, current and predicted need for oxygenation – possibly mismatched with supply due to a stressor – also inform respiration timings and their variations [3]–[5].

Despite widespread acknowledgement of this functional coupling between the central nervous system and respiratory physiology, studies of respiration pattern variability (RPV) have yet to demonstrate correlations with *underlying neural activity* in the context of stress. It seems reasonable to expect, however, that RPV could capture information pertinent to functional neuroactivity during stress. Respiratory patterns will vary according to the demands of the central and autonomic nervous systems. Yet, the majority of research on RPV has bypassed this constituent step and has instead studied the direct relationship between stimulus presentation and these peripheral measures' responses [6]–[11]. Importantly, establishing such correspondence with functional neuroactivity would spur the development of RPV quantification methods toward neural engineering for stress – as has been done already for heart rate variability (HRV) [12], [13]. More diverse sets of markers would thereby be validated for tracking latent neurophysiological stress, which is especially relevant for those suffering from trauma and anxiety disorders (e.g., PTSD). The need for said demonstrative research thus remains.

In fact, to the best of our knowledge, the sole investigation of RPV and simultaneous functional neuroimaging thus far has been that of [14], where sinusoidal regularity in breathing demonstrated a positive association with connectivity between the cingulate cortex and hippocampus, as measured using functional magnetic resonance imaging. Although the work of [14] partially inspired this paper's analysis, it differs in its focus on RPV's relationship to default mode network connectivity and its deterioration in remitted depression, rather than functional neuroactivity during responses to stress-relevant stimuli in traumatized subjects. Respiration quality assessment was also not employed during signal processing. Indeed, the literature on RPV has paid inadequate attention to confounds related to signal deterioration, let alone leverage available electrocardiogram (ECG) signals via ECG-derived respiration for added robustness [15] – despite the inherent corruption of wearable respiration sensing by motion and tissue artifacts.

To address these limitations, 50 human subjects with prior traumatic experience (24 with posttraumatic stress disorder (PTSD)) were studied over the span of a 2–3

Author Manuscript Author Manuscript Author Manuscript Author Manuscript

hour-long protocol involving traumatic stress and transcutaneous cervical vagus nerve stimulation (tcVNS). Stimulus-induced responses were assessed using concurrent high-resolution positron emission tomography (HR-PET) for regional cerebral blood flow (rCBF) measurements and electrocardiogram (ECG) and belt-based respiratory effort (RSP) sensing to estimate peripheral cardiorespiratory physiological parameters. Utilizing automated signal processing algorithms, respiratory variability was extracted and evaluated for its neurophysiological significance in the context of traumatic stress and tcVNS via a 1) correlation analysis with limbic brain activity and 2) active vs. sham tcVNS comparisons, as illustrated in Fig. 1.

This enabled evaluation of the following hypotheses:

H1) RPV will add value in capturing the latent ANS and limbic system variations induced by traumatic stressors and tcVNS – notably not already captured by HRV. Secondarily, we hypothesized that correlated variability in breathing would inversely relate to distress, as in [7]–[11].

H2) Based on the withdrawal and enhancement of vagal tone during inspiration and expiration, respectively [6], extracting inspiration and expiration times will better enable quantification of tcVNS effects on RPV than that afforded by the coarser measure of respiration rate.

These hypotheses guided our assessment of RPV's potential utility as a marker for quantifying neurorespiratory variations and informing therapeutic interventions.

We consequently make the following contributions to the state of the art:

C1) Establish the potency of respiratory variability in quantifying the underlying central and autonomic nervous system responses to traumatic stress and tcVNS

C2) Demonstrate that constituent inspiration and expiration times are necessary to capture tcVNS effects

C3) Design and elucidate an end-to-end respiration processing and variability extraction pipeline that incorporates both RSP and ECG-derived respiration signals with validated respiration quality assessment

To enhance utility and foster reproducibility, all processing and variability extraction code has been made available at https://github.com/asimgazi24/RespProcessing_RPV.

II. Methods

A. Study Protocol and Population

On the first morning of a three-day protocol (ClinicalTrials.gov identifier NCT02992899) approved by the Institutional Review Boards of the Georgia Institute of Technology (#H17126), Emory University School of Medicine (#IRB00091171), SPAWAR Systems Center Pacific, and the Department of Navy Human Research Protection Program, 50 human subjects (32 females) with a mean age of 34 (SD 11) years and body mass index (BMI) of 27 (SD 5) participated in a concurrent physiological sensing and functional neuroimaging study involving a series of 10 stimuli, as chronologically depicted in Fig. 2. All recording

Author Manuscript Author Manuscript Author Manuscript Author Manuscript

considered in this work occurred at ~20° C between the hours of 9:00 and 13:00 – prior to the uncontrolled lunch break provided to the participants. This reduced the potential confounding effects of circadian rhythm- and meal intake-induced variability in peripheral and neuro-physiological responses [16], [17]. Participants were instructed to refrain from any stimulant use (e.g., caffeine) throughout the duration of the protocol and were further required to fast after 6:00.

To investigate traumatic stress-relevant variations in the subjects' peripheral and neural physiology, audible neutral or trauma scripts of 60-s length were played to the subjects via headphones in the ordering illustrated in Fig. 2. Neutral scripts comprised of descriptions of pleasant scenery meant to induce neutral or positive affect, while traumatic stress consisted of personalized narrations of prior trauma. All subjects had history of psychological trauma, but only 24 of the subjects were clinically diagnosed with PTSD at the time; the remaining 26 did not suffer from any severe psychiatric disorder. For further details specific to either modality or disease state the reader is referred to [18]–[21].

B. Double-Blind Stimulation

Adhering to a randomized double-blind clinical trial (ClinicalTrials.gov NCT02992899), each subject received only one of either active transcutaneous cervical vagus nerve stimulation (tcVNS) or sham stimulation at specified times illustrated in Fig. 2. Stimulation was delivered to the cervical portion of the left vagus nerve for 120 s after each of the four traumatic stressors, as well as twice separately to assess stimulation-specific effects. The active and sham devices (gammaCore, electroCore, Basking Ridge, NJ, USA) appeared and operated identically, differing only in stimulation parameters [19].

C. Physiological Sensing

Respiratory effort (RSP) and electrocardiogram (ECG) signals were measured at the locations shown in Fig. 1 using the Biopac RSPEC-R system (Biopac Systems, Goleta, CA, USA) from subjects lying supine inside a high-resolution positron emission tomography (HR-PET) scanner. RSP was transduced using a belt measuring thoracic expansion and contraction via a strain gauge, while ECG was measured using adhesive Ag/AgCl electrodes in a three-lead configuration. All data were acquired at a 2-kHz sampling rate using the Biopac MP150 16-bit data acquisition system.

D. Functional Neuroimaging

Brain perfusion during each protocol condition was measured using HR-PET imaging via a High Resolution Research Tomograph (CTI, Knoxville, TN); this enabled the quantification of regional voxel-wise activity at a 2-mm spatial resolution. Five seconds prior to audible script or electrical stimulation (scans 5 and 6), 20 mCi of radio-labeled water (H_2O^{15}) produced in an on-site cyclotron was intravenously administered. Subjects were then instructed to remain still for the duration of the scan to minimize motion artifact, and a 120-s HR-PET scan was initiated simultaneously with script presentation or stimulation. Each resultant image produced a single functional snapshot of coincident event counts localized to their respective voxels. As shown in Fig. 2, the inter-scan interval was ~ 500 s.

Author Manuscript Author Manuscript Author Manuscript Author Manuscript

E. Electrocardiogram Processing

Fig. 3 depicts the fully automated preprocessing, quality assessment, and timing extraction pipelines for ECG and respiration. Unless otherwise stated, all signal processing was performed in MATLAB (R2019b, Natick, MA), and all filtering was done both forward and backward using optimal Chebyshev finite impulse response (FIR) filters. For ECG, raw signals were first bandpass filtered with a passband of 0.6–40 Hz [22]. Then, an interim set of ECG R-peaks were detected using the Pan-Tompkins (PT) algorithm [23] – notably "interim" due to the infrequent, but nevertheless existent, deteriorations in ECG signal quality. For the sole purpose of detecting these corruptions, two additional annotation schemes were used to locate R peaks in parallel, [24], [25], from which two signal quality indices (SQI) were derived for each 10-s window of ECG data using F-scores [26]. For both F-scores, the PT algorithm was treated as the reference annotator, where peak times could differ by no more than 100 ms.

Letting the F-score computed between the algorithm of [25] and PT be $SQI_1(\cdot)$, the F-score computed between the algorithm of [24] be $SQI_2(\cdot)$, the window index be i, where $i \in \left\{1, 2, \ldots, \left\lfloor \frac{T}{10} \right\rfloor\right\}$, and T be the time length of data collected for the particular subject, windows of ECG data containing corrupted portions were removed as follows. Any window of index i such that $SQI_1(i) < 0.5$ was removed, unless one of two exceptions occurred: (1) $SQI_1 < 0.5$ for greater than 60 contiguous seconds within the subject's data, or (2) $\frac{1}{T}\sum_{i=1}^{T} SQI_1(i) < 0.85$. If either exception occurred, SQI_2 was instead used on the subject's data with a threshold of 0.7, i.e., any window of index i such that $SQI_2(i) < 0.7$ was removed. SQI_1 was hence treated as the default and SQI_2 served as an alternate – this decision was made following inspection of SQI_1, SQI_2 performance on the dataset at hand. All thresholds were empirically tuned based on the dataset characteristics and the desired sensitivity / specificity in detecting corrupted windows of ECG data; thus, for alternate applications, the specific numerical thresholds may need modification [26].

From the remaining windows, the PT R peaks were stored, and R-R intervals were computed by finding the time, in ms, between all R peak pairs lying entirely within ECG windows of sufficient quality. Note here that the time corresponding to the second peak of each pair was stored alongside these R-R intervals for forthcoming reasons. Any outlier (greater than ± 4 SD from the mean) or physiologically unlikely (> 2000 ms (30 bpm) or < 400 ms (150 bpm)) R-R intervals were then removed, along with their corresponding second peak times. For subjects with evident arrhythmias, this final step was replaced with two-stage outlier removal to eliminate arrhythmic beats. Specifically, R-R intervals further than ± 3 median absolute deviations (MADs) from the overall median were removed, followed by 30-element moving window outlier removal with ± 2 MAD bounds away from the window-specific medians. These steps resulted in a final set of "clean" R-R intervals, or what will be referred to as normal-to-normal (NN) intervals [27]. These quality assessment steps resulted in the removal of 3 (SD 7) % of the ECG data; this mean and SD include subjects with arrhythmias. Data removal was estimated by dividing the number of datapoints within NN intervals by the total number of raw ECG datapoints available.

Author Manuscript Author Manuscript Author Manuscript Author Manuscript

F. Respiration Processing

For respiration processing, the belt-based signal was supplemented with two additional ECG-derived respiration signals: the respiration-induced intensity variation (RIIV) and the respiration-induced amplitude variation (RIAV) [28]. RIIV and RIAV were extracted by leveraging the original raw ECG signal, the NN intervals, denoted $NNI = [nni_1, nni_2, \ldots, nni_N]$, and the corresponding second R peak times, denoted $S = [s_1, s_2, \ldots, s_N]$. In particular, NNI and S were first used to compute a final set of clean R peak times, C, by subtracting NN intervals from their corresponding second peak times and then appending the final second peak time, s_N, to the difference, i.e., $C = [(S - NNI), S_N] \in \mathbb{R}^{N+1}$. R peak values were then determined by finding the raw ECG values corresponding to these clean R peak times, C. This resultant vector of R peak values forms the RIIV signal. RIAV is then derived by finding the ECG R peak amplitudes; each amplitude is calculated by computing the difference between R peak value and the minimum ECG value within 100 ms prior. Although respiration quality-oriented work involving ECG-derived respiration typically utilizes the respiration-induced frequency variation (RIFV) signal as well [15], deteriorated respiratory sinus arrhythmia (i.e., insufficient frequency modulation) precluded its use in this study [29].

To preprocess and extract an interim set of inter-breath intervals (IBIs) and breath onsets from these three respiration signals, RSP, RIIV, and RIAV were first linearly resampled to 50 Hz with an antialiasing low-pass filter, followed by bandpass filtering with passband 0.1 – 0.72 Hz (6 – 43 bpm). The filtered signals were then windowed (60-s width, 2-s overlap) for adaptive thresholding, where peaks were detected within each window by enforcing a minimum peak prominence of half of the window's standard deviation and a minimum time between peaks of 1.4 s, as in [14]. Respiration onsets were then determined by first computing IBIs using these peaks, keeping track of time as done with R-R intervals, and locating the minimum value within the time window corresponding to each IBI. The result is thus a paired set of IBIs and onsets.

Respiration quality assessment and feature-level fusion were then performed by reverting to the original RSP, RIIV, and RIAV signals themselves, resampling to 4 Hz, and equivalently bandpass filtering (0.1 – 0.72 Hz). A respiration quality index (RQI) is then computed for each 16-s non-overlapping window of filtered data (indexed here by $j \in \left\{1, 2, \ldots, \left\lceil \frac{T}{16} \right\rceil\right\}$) – normalized to zero mean, unit variance – by taking the mean of two respiration quality indices (RQIs) adapted from prior literature [30]. Specifically, we employed a power spectral density (PSD)-based RQI, $rqi_1(\cdot)$, where the PSD was estimated using a 64-point fast Fourier transform (FFT) that returned a vector of components, $F(j) \in \mathbb{R}^{33}$, corresponding to power within each frequency bin of resolution $\frac{1}{16}$ Hz (ignoring the DC component). $rqi_1(j)$ was then computed using (1),

$$rqi_1(j) = \frac{\max\limits_{z \in \{3,4,\ldots,17\}} \sum_{i=z-1}^{i=z} F_i(j)}{\sum_{i=3}^{33} F_i(j)} \tag{1}$$

Author Manuscript Author Manuscript Author Manuscript Author Manuscript

where z was limited according to [30]. An autocorrelation based RQI $rqi_2(\cdot)$ was also employed, computed using (2),

$$rqi_2(j) = \frac{\max\limits_{l \in \{4,5,\ldots,48\}} \sum_{n=1}^{64-l} y_n(j) y_{n+l}(j)}{63\sigma_y^2(j)} \tag{2}$$

where $y(j) \in \mathbb{R}^{64}$ represents the 16-s window of respiration data resampled to 4 Hz, and $\sigma_y(j)$ represents the standard deviation of $y(j)$. The final RQI for each window is computed as $RQI(j) = \frac{1}{2}(rqi_1(j) + rqi_2(j))$. This windowing and respiration quality indexing is performed separately for each of the three signals.

With each signal's set of 16-s window-specific RQIs stored, the previously computed IBIs and onsets are fused in a manner that assures both quality and the preservation of respiration data. In particular, the IBIs and onsets corresponding to the signal with maximum RQI were then selected for each window, provided that one or more of the three signals' RQIs within the window remained above an empirically tuned threshold of $\tau = 0.45$. This produced fused sets of IBIs and onsets, from which any implausible IBIs (> 10 s (6 bpm) or < 1.4 s (43 bpm)), and corresponding onsets, were removed. Note that for windows with ECG data deemed unusable by SQI, only the belt signal was considered.

With fused IBIs and breath onset times in hand, an interim set of respiration timing features were extracted for further amelioration of unacceptable data, leveraging outlier detection. Inspiration time (T_i), expiration time (T_e), and respiration rate (RR) are computed as the time difference (in seconds) between second peak of the IBI and corresponding onset, first peak of the IBI and the onset, and 60 multiplied by the reciprocal of the IBI, respectively; the IBI peaks were computed in a manner akin to how the NN intervals were used to find clean ECG R peaks earlier.

Using each of the three resultant time series, three sets of flagged IBI and onset indices were produced, corresponding to RR, T_i, and T_e values that were deemed outliers using a two-stage outlier flagging approach. More specifically, if we let $IBI = \{ibi_1, ibi_2, \ldots, ibi_N\}$ represent the set of fused IBIs, $O = \{o_1, o_2, \ldots, o_N\}$ represent the set of fused onset times, $RR = [rr_1, rr_2, \ldots, rr_N]$ represent the computed RR, $T_i = [t_{i_1}, t_{i_2}, \ldots, t_{i_N}]$ represent T_i, and $T_e = [t_{e_1}, t_{e_2}, \ldots, t_{e_N}]$ represent the resultant T_e, then we flag outliers and remove IBIs and onsets as follows. First, for RR, T_i, and T_e, all indices corresponding to values lying outside ± 4 MAD away from the overall median are flagged, where, for example, if rr_j is flagged as an outlier, the index j is appended to a set of indices corresponding to RR outlier indices, $\theta_{RR} \subset \{1, 2, \ldots, N\}$. The same is done for Ti to produce $\theta_{Ti} \subset \{1, 2, \ldots, N\}$ and T_e to produce $\theta_{Te} \subset \{1, 2, \ldots, N\}$. θ_{RR}, θ_{T_i}, θ_{T_e} are then further appended to using a second stage of 30-element moving window outlier flagging applied to RR, T_i, and T_e, respectively, where indices corresponding to values lying outside ± 4 MADs from the window-specific medians are flagged. A single set of outlier indices, Θ, is then generated by taking the union of θ_{RR}, θ_{T_i}, and θ_{T_e}, i.e., $\Theta = \theta_{RR} \cup \theta_{T_i} \cup \theta_{T_e}$. The "clean" IBIs, IBI^*, and onsets, O^*, can

Author Manuscript Author Manuscript Author Manuscript Author Manuscript

then be produced by keeping only the IBIs and onsets of indices corresponding to the set difference, i.e.,

$$IBI^* = \{ibi_n \mid n \in \{1, 2, \ldots, N\} \backslash \Theta\} \tag{3}$$

$$O^* = \{o_n \mid n \in \{1, 2, \ldots, N\} \backslash \Theta\}. \tag{4}$$

From IBI^* and O^*, the final RR, Ti, and Te time series were once more computed using the methods aforementioned. Importantly, for both ECG and respiration processing, data removal takes place at the feature level, i.e., if a window of signal is deemed unsatisfactory, then the features extracted from the window are ignored. Thus, feature extraction is not affected by signal discontinuities.

These quality assessment steps resulted in the removal of 26 (SD 10) % of respiration data; notably, this removal increases to 41 (SD 16) % if ECG-derived respiration is ignored. This removal of 26 (SD 10) % aligns with prior literature [31]. Analogous to ECG, data removal was estimated by dividing the number of datapoints within "clean" IBIs by the total number of raw RSP datapoints available.

G. Respiratory and Heart Rate Variability

For each of the three respiration time series features, RR, T_i, and T_e, four RPV metrics were computed based on prior literature to quantify various aspects of the time series' fluctuations throughout the protocol [7]–[11], [14], [32]: the unscaled autocorrelation function (ACF) at one time lag, $\widetilde{\mathrm{ACF}}_{(\cdot)}(1)$, the scaled ACF at one time lag $\mathrm{ACF}_{(\cdot)}(1)$, the coefficient of variation (CV), CV(·), and the root mean square of successive differences (RMSSD), RMSSD(·). This totals to 12 RPV features. Each of these RPV features is computed on a rolling window basis, where window length is set to 300 s and overlap is set to 299 s. Hence, the resultant RPV features form new time series with inter-sample intervals of 1 s, where the time point associated with each value is set to be the center of the window. Fig. 4 depicts the overall computation process for a single window of example RR data from a subject.

If we let $X = [x_1, x_2, \ldots, x_N]^T$ represent a 300-s window of either RR, T_i, or T_e, then the four corresponding RPV metrics can be computed for this window as follows. For the ACF metrics at one time lag, we first define $X_{-1} = [x_2, x_3, \ldots, x_N]^T$ and $X_{-N} = [x_1, x_2, \ldots, x_{N-1}]^T$. Then, the unscaled ACF at one time lag can be computed as

$$\widetilde{\mathrm{ACF}}_X(1) = X_{-1}^T X_{-N}, \tag{5}$$

and the scaled ACF at one time lag can be computed as

$$\mathrm{ACF}_X(1) = \frac{X_{-1}^T X_{-N}}{X^T X}. \tag{6}$$

RMSSD also makes use of X_{-1} and X_{-N}; specifically

Author Manuscript Author Manuscript Author Manuscript Author Manuscript

$$\mathrm{RMSSD}(X) = \sqrt{\frac{(X_{-1} - X_{-N})^T (X_{-1} - X_{-N})}{N}}. \tag{7}$$

Finally, CV is computed by taking the standard deviation of the window and dividing it by the window's mean, i.e., letting

$$\mu_X = \frac{1}{N}\sum_{i=1}^{N} x_i \text{ and } \sigma_X = \sqrt{\frac{1}{N-1}\sum_{i=1}^{N}(x_i - \mu_X)^2}, \quad \mathrm{CV}(X) = \frac{\sigma_X}{\mu_X}. \tag{8}$$

Heart rate variability (HRV) features were also computed on a 300-s rolling window basis with 299-s overlap using the NN intervals. Utilizing the PhysioNet Cardiovascular Signal Toolbox [33], the following HRV features were extracted due to their demonstrated relevance to stress [34]: RMSSD, pNN50, LF/HF, and SD1/SD2. The final HRV feature extracted was respiratory sinus arrhythmia (RSA), computed using the Porges-Bohrer method [35].

H. Neuroimage Processing and Segmentation

Using statistical parametrical mapping (SPM12; www.fil.ion.ucl.ac.uk/spm), HR-PET images were processed as in previous research [18]. First, a mean intensity image was generated using the individual scans. Then, the individual scans were spatially normalized to this mean intensity image, transformed into a common anatomical space (SPM PET Template), and smoothed using a 3-D Gaussian filter at 5-mm full width half maximum. To then assess relative activations and deactivations over the protocol time course, the individual images were total count normalized to whole brain activity.

Operating under the hypothesis that limbic brain activity would be most relevant given the extensive literature implicating these regions in fear, trauma, and stress-related responses [36], we segmented and studied 14 particular areas – seven from each hemisphere. These seven were the amygdala, hippocampus, anterior cingulate cortex (ACC), midcingulate cortex (MCC), insula, thalamus, and rostromedial prefrontal cortex (rmPFC). For all regions but the rmPFC, segmentation was performed on the total-count-normalized images by leveraging the automated anatomical labeling (AAL) atlas [37]; for the rmPFC, custom masks derived from the AAL atlas's inferior half of the superior medial frontal gyrus were used [38]. This resulted in regional cerebral blood flow (rCBF) estimates for 14 brain areas during each of the 10 protocol conditions. For further details on each of the brain regions, please see the supplementary material.

I. Identifying Neural Correlates

For each of the RPV, HRV, and additional features that were deemed extraneous to the significance of this work (detailed in the supplementary material), resampling to 1 Hz, moving window averaging with a 5-s window, and segmentation to protocol condition first took place similarly to the time series preparation of prior work [39]. In this case, however,

Author Manuscript Author Manuscript Author Manuscript Author Manuscript

segmentation corresponded to only to the first 60 s of each HR-PET scan. This was in accordance with prior correlation analyses utilizing O15 water-based PET imaging, where the tracer uptake period is of pertinence (e.g., [40], [41]). Once the features were segmented, the mean was computed for each of the conditions, corresponding to 10 mean values for each of the peripheral physiological features, corresponding to the 10 sets of brain activity measures previously stored (in the maximal case, i.e., no data missing).

With this correspondence established, correlations between each brain area-physiological feature pair were analyzed using linear mixed effects (LME) modeling in R using the lme4 package [42]. Unless otherwise stated, the non-PTSD and PTSD groups were treated separately given the notable psychophysiological deteriorations well-documented in the literature for those suffering from PTSD [43]. Each LME model investigated the relationship between one of the physiological features and one of the brain areas for each disease state, where brain activity was treated as the dependent variable and physiological measure as the independent variable and sole fixed effect. Subjects were included as random effects to adequately account for the repeated measures for each subject, providing increased statistical power over approaches such as the Fisher transform for aggregation [40]; both subject-specific slopes and intercepts were included [44]. The models were fit using maximum likelihood estimation with unstructured covariance, whereafter, residual plots were investigated for homoscedasticity and normality – no obvious deviations were observed. P-values were then obtained using likelihood ratio tests (LRTs) of the full model with physiological measure as a fixed effect vs. the model without this effect in question [45], [46]. Chi square values correspond to the LRT statistic.

Significant correlates were identified by enforcing $P<1.37\times10^{-4}<\frac{.05}{26\times14}$. This conservative Bonferroni correction factor of 26 × 14 was determined using the number of related comparisons performed over the entirety of the feature set, including the extraneous features omitted from the main manuscript (supplementary material).

J. Comparing Active vs. Sham Stimulation Responses

Upon finding significant neural correlates, respiratory variability was then evaluated for its relevance to tcVNS-induced effects. To investigate this, the active vs. sham analysis steps taken in our group's prior work were mirrored with the variability features of interest [19]. First, each feature time series was normalized as a relative percent difference from a subject-specific baseline, where the baseline was computed by finding the average value across the first minute of the subject's available data within the 240 s prior to the first neutral script. Note that in the sole case of pNN50, normalization was done without division to account for the 0% baselines of certain subjects. These normalized time series were then segmented according to intervals of interest: the first 30 s of traumatic recall, first minute of stimulation, last minute of stimulation, and one minute from post-stimulation, starting from 3 minutes after stimulation stopped (i.e., interval of [180, 240] s after stimulation; the first minute was additionally included based on the results of our group's prior state-space modeling work [39]. Fig. 2 illustrates the ordering of these intervals for each stimulation condition. Responses following traumatic stress were analyzed separately from responses with no prior stress, and the PTSD group was again analyzed separately from the non-PTSD

Author Manuscript Author Manuscript Author Manuscript Author Manuscript

group. To return one value per interval for each subject, values of the same interval type were averaged. These sets of subject-specific percent changes were then compared between the active and sham groups for each of the intervals under study.

Due to the absence of normality precluding the use of multivariate analysis of variance (MANOVA) in comparing the groups, two-tailed Mann-Whitney U tests or independent t-tests were employed for variables with nonnormally and normally distributed residuals, respectively (tested with Shapiro-Wilk test). If equality of variance was rejected (tested with Levene's test) for a variable with normally distributed residuals, Welch's independent t-test was used; otherwise, Student's t-test was used. The level of significance was set to $\alpha = \frac{.05}{3}$ to account for three comparisons per feature. Effect sizes were computed using Cohen's d or the common language effect size, f, as appropriate.

III. Results

A. Variability Correlates of Limbic Brain Activity

Fig. 5 illustrates the significant variability correlates discovered for both the non-PTSD and PTSD groups. The variations in respiration rate captured via the unscaled autocorrelation function at one time lag, $\widetilde{\mathrm{ACF}}_{(RR)}(1)$, correlated positively with the right rmPFC ($P = 9.4 \times 10^{-5}$, $\chi^2(1) = 15.2$) and negatively with the left amygdala ($P = 7.6 \times 10^{-8}$, $\chi^2(1) = 28.9$) for the non-PTSD group – these areas are colored in blue. The fluctuations in NN intervals captured by the RMSSD exhibited a significant positive correlation with the left hippocampus ($P = 3.0 \times 10^{-5}$, $\chi^2(1) = 17.4$) for the non-PTSD group – this area is colored in red.

For the PTSD group, the only significant neural correlate detected was the $\widetilde{\mathrm{ACF}}_{(RR)}(1)$, which exhibited a positive correlation with the right rmPFC ($P = 5.5 \times 10^{-7}$, $\chi^2(1) = 25.1$) and negative correlations with both the left and right insulae ($P = 8.3 \times 10^{-5}$, $\chi^2(1) = 15.5$; $P = 1.2 \times 10^{-5}$, $\chi^2(1) = 19.2$, respectively). Also included in Fig. 5 are example time series plots from a single subject for both implicated variability features, as well as example correlation data and mixed model fits across all subjects in the non-PTSD group; subject ID is colored equivalently in the two spaghetti plots shown. The BrainNet Viewer was used for 3-D brain rendering [47], where additional views are provided as supplementary material.

B. Variability Differences Between Active and Sham tcVNS

Fig. 6 displays the significant differences found between relative responses to active and sham tcVNS. For the non-PTSD group, only an RPV metric differed significantly after correction: the unscaled ACF of expiration time at one time lag, $\widetilde{\mathrm{ACF}}_{(Te)}(1)$. Both with and without prior traumatic stress, the relative responses for the active group were higher than that of the sham group during the post-stimulation period ($P = .013$, $t = 2.8$, $d = 1.16$ without prior traumatic stress; $P = .016$, $U = 42$, $f = .25$ with prior traumatic stress). For the PTSD group, only HRV differed significantly, where two metrics not reported on previously in prior literature, RMSSD and pNN50, are shown. The RMSSD of NN intervals differed significantly during both the first and second minutes of stimulation ($P = .0005$, $U = 14$, f =

Author Manuscript Author Manuscript Author Manuscript Author Manuscript

.097; P = .001, U = 18, f = .13, respectively), while the pNN50 differed significantly only during the first (P = .01, U = 31, f = .22) – both were higher in the active group than in the sham group.

IV. Discussion

A. Respiratory Variability Correlates with Limbic Regions Implicated in Both Subconscious and Conscious Processes

In Fig. 5, the neural correlates of $\widetilde{\mathrm{ACF}}_{(RR)}(1)$ not only include limbic regions that primarily operate in the subconscious realm, but also areas that are believed to additionally play meaningful roles in consciousness [48]. This is an intriguing point considering respiration differs from most other physiological processes – modulation can occur both consciously and subconsciously. For the non-PTSD group, activity within the left amygdala and the right rmPFC correlated significantly with $\widetilde{\mathrm{ACF}}_{(RR)}(1)$; in the PTSD group, this same metric exhibited correlations, again, with the right rmPFC, as well as two additional areas: the left and right insulae. The left amygdala has been implicated in numerous subconscious functions pertinent to autonomic regulation, emotional responses, and memory processing [49]. The rmPFC and insula have similarly been implicated in subconscious autonomic regulation and emotional responses [50], [51]. Specifically for the insula and rmPFC, however, prior work has also demonstrated their importance in social interaction, autobiographical history (critical to traumatic stress responses), and conscious awareness in the present [51]–[53]. Thus, respiration, autonomic regulation, and mindfulness are demonstrably intertwined, and the neural correlates reported herein suggest that respiratory variability can play an enabling role in gauging the neural basis for these mind-body phenomena.

B. Correlation Directions Suggest Correlated Variability in Respiration Rate Inversely Relates to Distress

The correlation directions shown in Fig. 5 seem to suggest that increases in $\widetilde{\mathrm{ACF}}_{(RR)}(1)$ indicate reduced distress. For the non-PTSD group, $\widetilde{\mathrm{ACF}}_{(RR)}(1)$ correlated positively with right rmPFC activity and negatively with left amygdala activity. A simultaneous positive correlation with the right rmPFC and negative correlation with the left amygdala could imply that correlated variability in respiration rate is associated with increases in top-down regulation of amygdala fear responses via medial prefrontal cortex activity [49], [54]. For the PTSD group, the right rmPFC, again, positively correlated with $\widetilde{\mathrm{ACF}}_{(RR)}(1)$, while activity in the insula negatively correlated with $\widetilde{\mathrm{ACF}}_{(RR)}(1)$. Although the insula (and amygdala, for that matter) is involved in both negative and positive affective responses, in this study focused on traumatic stress, decreases in activity are generally considered a positive outcome [18]. Therefore, in line with findings from previous RPV research [1], [7]–[11], decreased correlated variability in breathing seems to entail undesirable distress during traumatic recall.

Author Manuscript Author Manuscript Author Manuscript Author Manuscript

C. tcVNS Increases Post-Stimulation Correlated Variability in Expiration Time for Subjects Without PTSD

The significant increase in $\widetilde{\mathrm{ACF}}_{(Te)}(1)$ shown in Fig. 6 for the non-PTSD active vs. sham comparison suggests that tcVNS induces a post-stimulation increase in the correlated variability of exhalation in subjects without PTSD time (please see the appendix for a quantitative interpretation of "correlated variability," i.e., $\widetilde{\mathrm{ACF}}_{(\,\cdot\,)}(1)$). This aligns with expectation given that irregular breathing remains one of the characteristic respiratory responses to distress [1] – so regularity could indicate decreased distress. Moreover, PNS activity decreases during inspiration and increases during expiration due to respiratory sinus arrhythmia; thus, increased expiration time relative to inspiration time is strongly related to enhanced PNS activity relative to SNS activity [55]. Since tcVNS is purported to tilt sympathovagal balance toward heightened PNS activity relative to SNS activity, increased correlated variability in expiration could exist as one manifestation of the peripheral PNS-favoring exhalation effects of tcVNS.

D. Inspiration and Expiration Times Provide Information not Captured by Respiration Rate

Fig. 6 presents a notable absence of respiration rate variability. Our group has consistently found that the constituent inspiration and expiration timings add value beyond what respiration rate can provide on its own. In related efforts leveraging the processing methods of this work, we have found that the expiration time, itself, is lengthened by active tcVNS in comparison to sham for non-PTSD subjects [56]. Moreover, heightened inspiration to expiration time ratios were associated with increased apnea-hypopnea indices in individuals affected by sleep apnea [57]; notably, no significant correlations were observed with respiration rate. Extracting inspiration and expiration times on a breath-by-breath basis thus enables a more granular analysis of sympathovagal balance than that afforded by solely using the coarser measure of respiration rate.

E. Respiratory Variability Holds Value Distinct from HRV

As seen in both Fig. 5 and Fig. 6, RPV metrics contributed separate value from that of which HRV put forth. Namely, the HRV metric RMSSD(NN) correlated significantly with left hippocampal activity in the non-PTSD group, even though no RPV metric did the same. On the other hand, the RPV metric $\widetilde{\mathrm{ACF}}_{(RR)}(1)$ correlated significantly with multiple areas in both the non-PTSD and PTSD groups, but no HRV metric exhibited similar correlations. Moreover for the active vs. sham tcVNS comparisons, no HRV metric was found to differ significantly between the active and sham non-PTSD groups in previous work [19], and neither in the results reported herein; $\widetilde{\mathrm{ACF}}_{(Te)}(1)$ did, however, differ significantly. Meanwhile, for the PTSD group, numerous HRV metrics differed between the active and sham groups [20], including RMSSD and pNN50 reported here, but no RPV metrics were found to differ. This demonstrates the importance of considering RPV as its own dimension, separate from HRV, especially when studying traumatic stress and VNS.

Author Manuscript Author Manuscript Author Manuscript Author Manuscript

F. Limitations and Future Work

A few limitations are to be noted for this study. Although the general quantification of RPV possesses strong anatomical and physiological underpinnings (supplementary material), the interpretation of each metric in context remains slightly ambiguous (i.e.., is it healthy for this specific metric to increase or decrease?) [1], [8]–[11]. This is partly due to the sparsity in literature relative to other commonly used metrics (e.g., HRV). Results such as the ones detailed herein can therefore prompt others to consider RPV in related applications and thereby further the field's understanding.

Given this slight interpretation-related ambiguity, it was purposefully decided to exclude more complex variability metrics such as those recently explored for HRV (e.g., entropy [33]). Although such measures can provide additional value, the present analysis was restricted to measures that facilitated more straightforward quantitative interpretation. Further complexities could also have been included in the statistical models; however, the purpose of this study was to rigorously demonstrate that RPV adds significant value to ANS and limbic system related applications such as stress and VNS – not to identify all possible correlates. Future work can thus build upon these findings and explore added complexities.

A final note is the lack of any quantitative comparisons between the PTSD and non-PTSD groups. Due to the sample sizes of this study, more assertive inferences would amount to speculation, as clinical relevance is obtained with much larger samples. Nevertheless, the results presented herein suggest comparisons of RPV between individuals with and without PTSD to be a worthy investigation for future work.

V. Conclusion

This analysis demonstrates the utility of RPV in assessing underlying responses to traumatic stress and tcVNS. Leveraging both RSP and ECG-derived respiration signals, RPV features were robustly extracted and analyzed over the duration of a ~3-hr, 10-stimuli protocol involving personalized traumatic recall and tcVNS. By studying the limbic brain and RPV responses for 26 non-PTSD and 24 PTSD subjects, new correspondences were discovered. Specifically, the single-lag unscaled autocorrelation of respiration rate correlated negatively with the left amygdala and positively with the right rmPFC for the non-PTSD group; this same metric also correlated negatively with left and right insulae and positively with the right rmPFC for the PTSD group. Furthering this investigation, RPV responses to active and sham tcVNS were also compared, where the single-lag unscaled autocorrelation of expiration time was found to be significantly greater following stimulation in the active group compared to the sham group for non-PTSD subjects.

These findings suggest that respiratory variability underlies neurorespiratory responses to traumatic stress and neuromodulation. For sensing systems looking to improve estimates of latent physiological responses, the conventional HRV and skin conductance measurements should be supplemented with others including RPV to arrive at a more complete set of observables. For therapeutic interventions, targeting the respiratory center could serve well in regulating undesirable mind-body responses. Especially for those suffering from conditions such as PTSD and panic disorder where system state can alter drastically in a

Author Manuscript Author Manuscript Author Manuscript Author Manuscript

short period of time, closed-loop systems that consider variations in breathing patterns could importantly enhance quality of life.

Supplementary Material

Refer to Web version on PubMed Central for supplementary material.

Acknowledgments

The work of A. H. Gazi was supported by a National Science Foundation Graduate Research Fellowship (DGE-1650044). This research was supported by the Defense Advanced Research Projects Agency (N66001-16-4054 and N66001-19-2-4002) and the National Institutes of Health (UG3 DA048502 and R01 MH120262). The active and sham vagus nerve stimulation devices used in this research were provided free of charge by electroCore, Inc. Any opinion, findings, and conclusions or recommendations expressed in this material are those of the authors and do not necessarily reflect the views of the National Science Foundation, Defense Advanced Research Projects Agency, or National Institutes of Health.

Appendix

Analytically Dissecting the Unscaled Autocorrelation

The unscaled autocorrelation at one time lag, $\widetilde{\mathrm{ACF}}_{(\,\cdot\,)}(1)$, contributed to both the correlation analysis and active vs. sham results; as seen in Fig. 5 and Fig. 6, this was not the case for the scaled autocorrelation at one time lag, $\mathrm{ACF}_{(\cdot)}(1)$. This suggests that a lack of scaling provides some relevant measure of variability; thus, an analytic comparison of the two is in order. Noting that $\widetilde{\mathrm{ACF}}_{(\,\cdot\,)}(1) = \mathrm{ACF}_{(\,\cdot\,)}(1) \times \widetilde{\mathrm{ACF}}_{(\,\cdot\,)}(0)$, we find that $\widetilde{\mathrm{ACF}}_{(\,\cdot\,)}(0)$ acts as the scaling factor that differs between the two. Decomposing $\widetilde{\mathrm{ACF}}_{(\,\cdot\,)}(0)$, we have for a data window of length N, $X = [x_1, x_2, \ldots, x_N]$, $\widetilde{\mathrm{ACF}}_{(X)}(0) = X^T X = \sum_{i=1}^{N} x_i^2 = \sum_{i=1}^{N} (x_i - \mu_X + \mu_X)^2$, where $\mu_X = \frac{1}{N}\sum_{i=1}^{N} x_i$ is the mean of X. Therefore,

$$\widetilde{\mathrm{ACF}}_{(X)}(0) = \sum_{i=1}^{N}\left[(x_i - \mu_X)^2 + \mu_X^2 + 2\mu_X(x_i - \mu_X)\right] = N\sigma_X^2 + N\mu_X^2 + 2\mu_X\sum_{i=1}^{N}(x_i - \mu_X),$$
$$= N\left(\sigma_X^2 + \mu_X^2\right)$$

where $\sigma_X^2 = \frac{1}{N}\sum_{i=1}^{N}(x_i - \mu_X)^2$ is the population variance. Thus, $\widetilde{ACF}_{(\,\cdot\,)}(1) = N\left(\sigma_X^2 + \mu_X^2\right)ACF_{(\,\cdot\,)}(1)$, implying that the explanatory scaling factor is the product of the number of datapoints in the window and the sum of the mean squared and the variance. Hence, this metric in the context of RPV not only quantifies regularity in the respiratory feature, but also depends on RR, signal quality, and the window's first and second moments. Although these additional terms somewhat complicate interpretation, the demonstrated importance of $\widetilde{\mathrm{ACF}}_{(\,\cdot\,)}(1)$ provides support for multivariate fusion approaches.

References

[1]. Grossman P, "Respiration, Stress, and Cardiovascular Function," Psychophysiology, vol. 20, no. 3, pp. 284–300, 1983. [PubMed: 6408680]

[2]. Hall J, Guyton and Hall Textbook of Medical Physiology, 12th Editi. Philadelphia, PA: Elsevier, 2011.

Author Manuscript Author Manuscript Author Manuscript Author Manuscript

[3]. Ikeda K et al. , “The respiratory control mechanisms in the brainstem and spinal cord: integrative views of the neuroanatomy and neurophysiology,” Journal of Physiological Sciences, vol. 67, no. 1. Springer Tokyo, pp. 45–62, 01-Jan-2017.

[4]. Bartlett D and Leiter JC, “Coordination of breathing with nonrespiratory activities,” Compr. Physiol, vol. 2, no. 2, pp. 1387–1415, Apr. 2012. [PubMed: 23798304]

[5]. Herrero JL, Khuvis S, Yeagle E, Cerf M, and Mehta AD, “Breathing above the brain stem: Volitional control and attentional modulation in humans,” J. Neurophysiol, vol. 119, no. 1, pp. 145–159, Jan. 2018. [PubMed: 28954895]

[6]. Grassmann M, Vlemincx E, Von Leupoldt A, Mittelstädt JM, and Van Den Bergh O, “Respiratory changes in response to cognitive load: A systematic review,” Neural Plasticity, vol. 2016. Hindawi Limited, 2016.

[7]. Vlemincx E, Vigo D, Vansteenwegen D, Van den Bergh O, and Van Diest I, “Do not worry, be mindful: Effects of induced worry and mindfulness on respiratory variability in a nonanxious population,” Int. J. Psychophysiol, vol. 87, no. 2, pp. 147–151, Feb. 2013. [PubMed: 23266658]

[8]. Vlemincx E, Van Diest I, and Van den Bergh O, “Emotion, sighing, and respiratory variability,” Psychophysiology, vol. 52, no. 5, pp. 657–666, May 2015. [PubMed: 25524012]

[9]. Vlemincx E, Taelman J, De Peuter S, Van Diest I, and Van Den Bergh O, “Sigh rate and respiratory variability during mental load and sustained attention,” Psychophysiology, vol. 48, no. 1, pp. 117–120, Jan. 2011. [PubMed: 20536901]

[10]. Guyon AJAA et al. , “Respiratory Variability, Sighing, Anxiety, and Breathing Symptoms in Low- and High-Anxious Music Students Before and After Performing,” Front. Psychol, vol. 11, Feb. 2020.

[11]. Van Diest I, Thayer JF, Vandeputte B, Van de Woestijne KP, and Van den Bergh O, “Anxiety and respiratory variability,” Physiol. Behav, vol. 89, no. 2, pp. 189–195, Sep. 2006. [PubMed: 16859718]

[12]. Thayer JF, Åhs F, Fredrikson M, Sollers JJ, and Wager TD, “A meta-analysis of heart rate variability and neuroimaging studies: Implications for heart rate variability as a marker of stress and health,” Neuroscience and Biobehavioral Reviews, vol. 36, no. 2. Neurosci Biobehav Rev, pp. 747–756, Feb-2012. [PubMed: 22178086]

[13]. Rabellino D et al. , “Neural correlates of heart rate variability in PTSD during sub- and supraliminal processing of trauma-related cues,” Hum. Brain Mapp, vol. 38, no. 10, pp. 4898–4907, Oct. 2017. [PubMed: 28714594]

[14]. Zamoscik VE et al. , “Respiration pattern variability and related default mode network connectivity are altered in remitted depression,” Psychol. Med, vol. 48, no. 14, pp. 2364–2374, Oct. 2018. [PubMed: 29335031]

[15]. Charlton PH et al. , “Breathing Rate Estimation from the Electrocardiogram and Photoplethysmogram: A Review,” IEEE Rev. Biomed. Eng, vol. 11, pp. 2–20, Oct. 2018. [PubMed: 29990026]

[16]. Koch CE, Leinweber B, Drengberg BC, Blaum C, and Oster H, “Interaction between circadian rhythms and stress,” Neurobiology of Stress, vol. 6. Elsevier Inc, pp. 57–67, 01-Feb-2017. [PubMed: 28229109]

[17]. Johnston JD, “Physiological responses to food intake throughout the day,” Nutr. Res. Rev, vol. 27, no. 1, pp. 107–118, 2014. [PubMed: 24666537]

[18]. Wittbrodt MT et al. , “Non-invasive vagal nerve stimulation decreases brain activity during trauma scripts,” Brain Stimul, vol. 13, no. 5, pp. 1333–1348, Sep. 2020. [PubMed: 32659483]

[19]. Gurel NZ et al. , “Quantifying Acute Physiological Biomarkers of Transcutaneous Cervical Vagal Nerve Stimulation in the Context of Psychological Stress,” Brain Stimul, vol. 13, no. August, pp. 47–59, Jan. 2020. [PubMed: 31439323]

[20]. Gurel NZ et al. , “Transcutaneous cervical vagal nerve stimulation reduces sympathetic responses to stress in posttraumatic stress disorder: A double-blind, randomized, sham controlled trial,” Neurobiol. Stress, vol. 13, p. 100264, Nov. 2020. [PubMed: 33344717]

[21]. Wittbrodt MT et al. , “Non-Invasive Cervical Vagal Nerve Stimulation Alters Brain Activity During Traumatic Stress in Individuals with Posttraumatic Stress Disorder,” Brain Stimul.

Author Manuscript Author Manuscript Author Manuscript Author Manuscript

[22]. Sörnmo L and Laguna P, Bioelectrical Signal Processing in Cardiac and Neurological Applications, First Edit. Elsevier Inc., 2005.

[23]. Pan J and Tompkins WJ, "A Real-Time QRS Detection Algorithm," IEEE Trans. Biomed. Eng, vol. BME-32, no. 3, pp. 230–236, 1985.

[24]. Zong W, Moody GB, and Jiang D, "A robust open-source algorithm to detect onset and duration of QRS complexes," in Computers in Cardiology, 2003, vol. 30, pp. 737–740.

[25]. Engelse WAH and Zeelenberg C, "A single scan algorithm for QRS detection and feature extraction," in IEEE Computers in Cardiology, 1979, pp. 37–42.

[26]. Johnson AEW, Joachim B, Andreotti F, Clifford GD, and Oster J, "Multimodal heart beat detection using signal quality indices," Physiol. Meas, vol. 36, no. 8, p. 1665, 2015. [PubMed: 26218060]

[27]. Malik M et al. , "Heart rate variability: Standards of measurement, physiological interpretation, and clinical use," Circulation, vol. 93, no. 5, pp. 1043–1065, Mar. 1996. [PubMed: 8598068]

[28]. Karlen W, Raman S, Ansermino JM, and Dumont GA, "Multiparameter respiratory rate estimation from the photoplethysmogram," IEEE Trans. Biomed. Eng, vol. 60, no. 7, pp. 1946–1953, 2013. [PubMed: 23399950]

[29]. Campbell AA, Wisco BE, Silvia PJ, and Gay NG, "Resting respiratory sinus arrhythmia and posttraumatic stress disorder: A meta-analysis," Biol. Psychol, vol. 144, pp. 125–135, May 2019. [PubMed: 30779926]

[30]. Birrenkott DA, Pimentel MAF, Watkinson PJ, and Clifton DA, "A robust fusion model for estimating respiratory rate from photoplethysmography and electrocardiography," IEEE Trans. Biomed. Eng, vol. 65, no. 9, pp. 2033–2041, Sep. 2018. [PubMed: 29989939]

[31]. Charlton PH, Bonnici T, Tarassenko L, Clifton DA, Beale R, and Watkinson PJ, "An assessment of algorithms to estimate respiratory rate from the electrocardiogram and photoplethysmogram," Physiol. Meas, vol. 37, no. 4, pp. 610–626, Mar. 2016. [PubMed: 27027672]

[32]. Bruce EN, "Measures of Respiratory Pattern Variability," in Bioengineering Approaches to Pulmonary Physiology and Medicine, Springer US, 2007, pp. 149–159.

[33]. Vest AN et al. , "An open source benchmarked toolbox for cardiovascular waveform and interval analysis," Physiol. Meas, vol. 39, no. 10, Oct. 2018.

[34]. Giannakakis G, Grigoriadis D, Giannakaki K, Simantiraki O, Roniotis A, and Tsiknakis M, "Review on psychological stress detection using biosignals," IEEE Trans. Affect. Comput, pp. 1–1, Jul. 2019.

[35]. Lewis GF, Furman SA, McCool MF, and Porges SW, "Statistical strategies to quantify respiratory sinus arrhythmia: Are commonly used metrics equivalent?," Biol. Psychol, vol. 89, no. 2, pp. 349–364, Feb. 2012. [PubMed: 22138367]

[36]. LeDoux J, "Rethinking the Emotional Brain," Neuron, vol. 73, no. 4. pp. 653–676, 23-Feb-2012. [PubMed: 22365542]

[37]. Rolls ET, Huang CC, Lin CP, Feng J, and Joliot M, "Automated anatomical labelling atlas 3," Neuroimage, vol. 206, p. 116189, Feb. 2020. [PubMed: 31521825]

[38]. Moazzami K et al. , "Higher Activation of the Rostromedial Prefrontal Cortex during Mental Stress Predicts Major Cardiovascular Disease Events in Individuals with Coronary Artery Disease," Circulation, vol. 142, no. 5, pp. 455–465, Aug. 2020. [PubMed: 32522022]

[39]. Gazi AH et al. , "Digital cardiovascular biomarker responses to transcutaneous cervical vagus nerve stimulation: State-space modeling, prediction, and simulation," JMIR mHealth uHealth, vol. 8, no. 9, p. e20488, Sep. 2020. [PubMed: 32960179]

[40]. Liberzon I, Taylor SF, Fig LM, Decker LR, Koeppe RA, and Minoshima S, "Limbic activation and psychophysiologic responses to aversive visual stimuli: Interaction with cognitive task," Neuropsychopharmacology, vol. 23, no. 5, pp. 508–516, Nov. 2000. [PubMed: 11027916]

[41]. Lane RD, McRae K, Reiman EM, Chen K, Ahern GL, and Thayer JF, "Neural correlates of heart rate variability during emotion," Neuroimage, vol. 44, no. 1, pp. 213–222, Jan. 2009. [PubMed: 18778779]

[42]. Bates D, Mächler M, Bolker BM, and Walker SC, "Fitting linear mixed-effects models using lme4," J. Stat. Softw, vol. 67, no. 1, pp. 1–48, Oct. 2015.

Author Manuscript Author Manuscript Author Manuscript Author Manuscript

[43]. Bremner JD et al. , “MRI and PET study of deficits in hippocampal structure and function in women with childhood sexual abuse and posttraumatic stress disorder,” Am. J. Psychiatry, vol. 160, no. 5, pp. 924–932, May 2003. [PubMed: 12727697]

[44]. Barr DJ, Levy R, Scheepers C, and Tily HJ, “Random effects structure for confirmatory hypothesis testing: Keep it maximal,” 2013.

[45]. Winter B, “Linear models and linear mixed effects models in R with linguistic applications.”

[46]. Koch K-R, Parameter Estimation and Hypothesis Testing in Linear Models. Springer Berlin Heidelberg, 1999.

[47]. Xia M, Wang J, and He Y, “BrainNet Viewer: A Network Visualization Tool for Human Brain Connectomics,” PLoS One, vol. 8, no. 7, Jul. 2013.

[48]. Ledoux JE and Brown R, “A higher-order theory of emotional consciousness,” Proc. Natl. Acad. Sci. U. S. A, vol. 114, no. 10, pp. E2016–E2025, Mar. 2017. [PubMed: 28202735]

[49]. Barrett LF, Bliss-Moreau E, Duncan SL, Rauch SL, and Wright CI, “The amygdala and the experience of affect,” Soc. Cogn. Affect. Neurosci, vol. 2, no. 2, pp. 73–83, 2007. [PubMed: 18392107]

[50]. Kreplin U and Fairclough SH, “Activation of the rostromedial prefrontal cortex during the experience of positive emotion in the context of esthetic experience. An fNIRS study,” Front. Hum. Neurosci, vol. 7, no. DEC, Dec. 2013.

[51]. Critchley HD and Harrison NA, “Visceral Influences on Brain and Behavior,” Neuron, vol. 77, no. 4. Neuron, pp. 624–638, 20-Feb-2013. [PubMed: 23439117]

[52]. Craig AD, “How do you feel - now? The anterior insula and human awareness,” Nature Reviews Neuroscience, vol. 10, no. 1. Nature Publishing Group, pp. 59–70, Jan-2009. [PubMed: 19096369]

[53]. Cooper JC, Dunne S, Furey T, and O’Doherty JP, “Dorsomedial prefrontal cortex mediates rapid evaluations predicting the outcome of romantic interactions,” J. Neurosci, vol. 32, no. 45, pp. 15647–15656, Nov. 2012. [PubMed: 23136406]

[54]. Rosenkranz JA, Moore H, and Grace AA, “The Prefrontal Cortex Regulates Lateral Amygdala Neuronal Plasticity and Responses to Previously Conditioned Stimuli,” J. Neurosci, vol. 23, no. 35, pp. 11054–11064, Dec. 2003. [PubMed: 14657162]

[55]. Berntson GG, Cacioppo JT, and Quigley KS, “Respiratory sinus arrhythmia: Autonomic origins, physiological mechanisms, and psychophysiological implications,” Psychophysiology, vol. 30, no. 2, pp. 183–196, 1993. [PubMed: 8434081]

[56]. Gazi AH et al., “Transcutaneous Cervical Vagus Nerve Stimulation Lengthens Exhalation in the Context of Traumatic Stress,” in IEEE-EMBS International Conference on Biomedical and Health Informatics (BHI), 2021.

[57]. Perez-Alday EA et al. , “Severity of Obstructive Sleep Apnea is Associated with Stress-Induced Respiratory Sympathovagal Imbalance,” in Virtual SLEEP, 2021.

Author Manuscript Author Manuscript Author Manuscript Author Manuscript

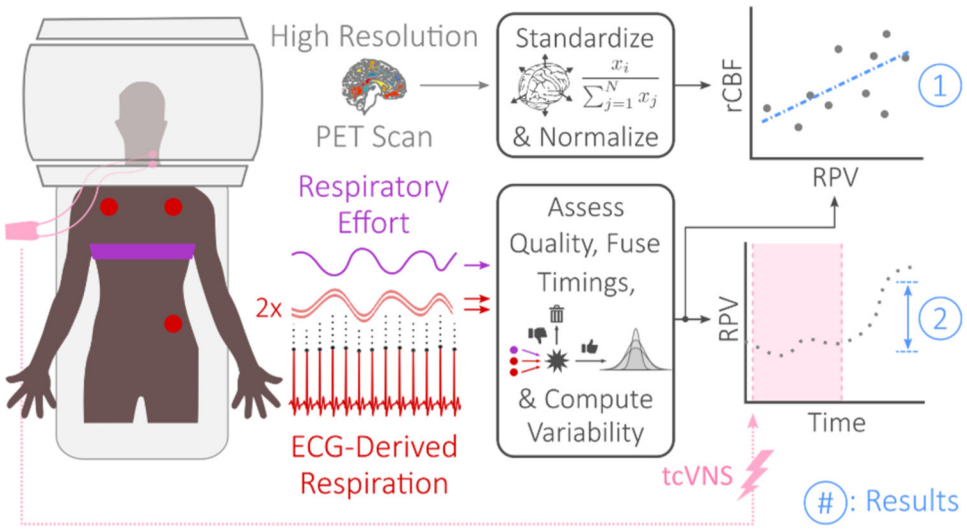

Fig. 1. High-Level overview of the analysis.

Respiratory effort and the electrocardiogram (ECG) were measured at the locations shown from subjects lying supine inside a high-resolution positron emission tomography (PET) brain scanner. Functional brain images were obtained during specified time windows to estimate regional cerebral blood flow (rCBF); transcutaneous cervical vagus nerve stimulation (tcVNS) was also administered at specified times. In this study, respiration pattern variability (RPV) measures are found to not only 1) significantly correlate with rCBF in key limbic regions, but are also 2) modulated significantly by tcVNS in comparison to a sham control.

Author Manuscript Author Manuscript Author Manuscript Author Manuscript

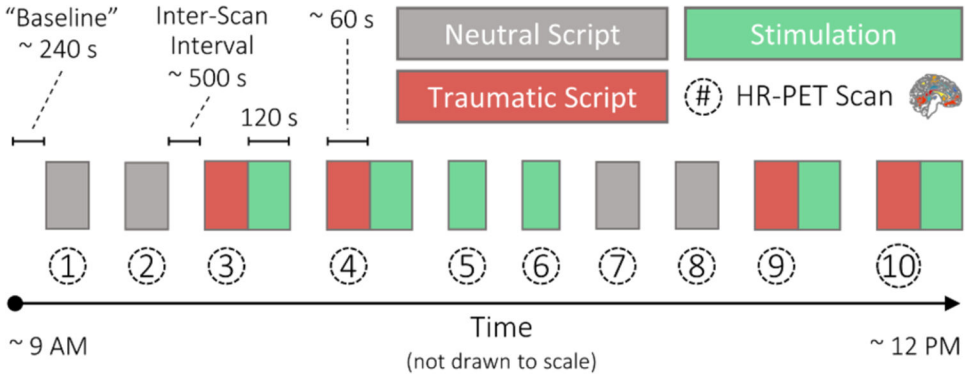

Fig. 2. Protocol diagram.

Subjects participated in a protocol of two to three hours in length involving neutral audio scripts, personalized traumatic audio scripts, and active transcutaneous cervical vagus nerve stimulation or sham stimulation administered for 120 s at a time. High-resolution positron emission tomography (HR-PET) brain scans were measured during the first two minutes of each stimulus condition to estimate functional neuroactivity.

Author Manuscript Author Manuscript Author Manuscript Author Manuscript

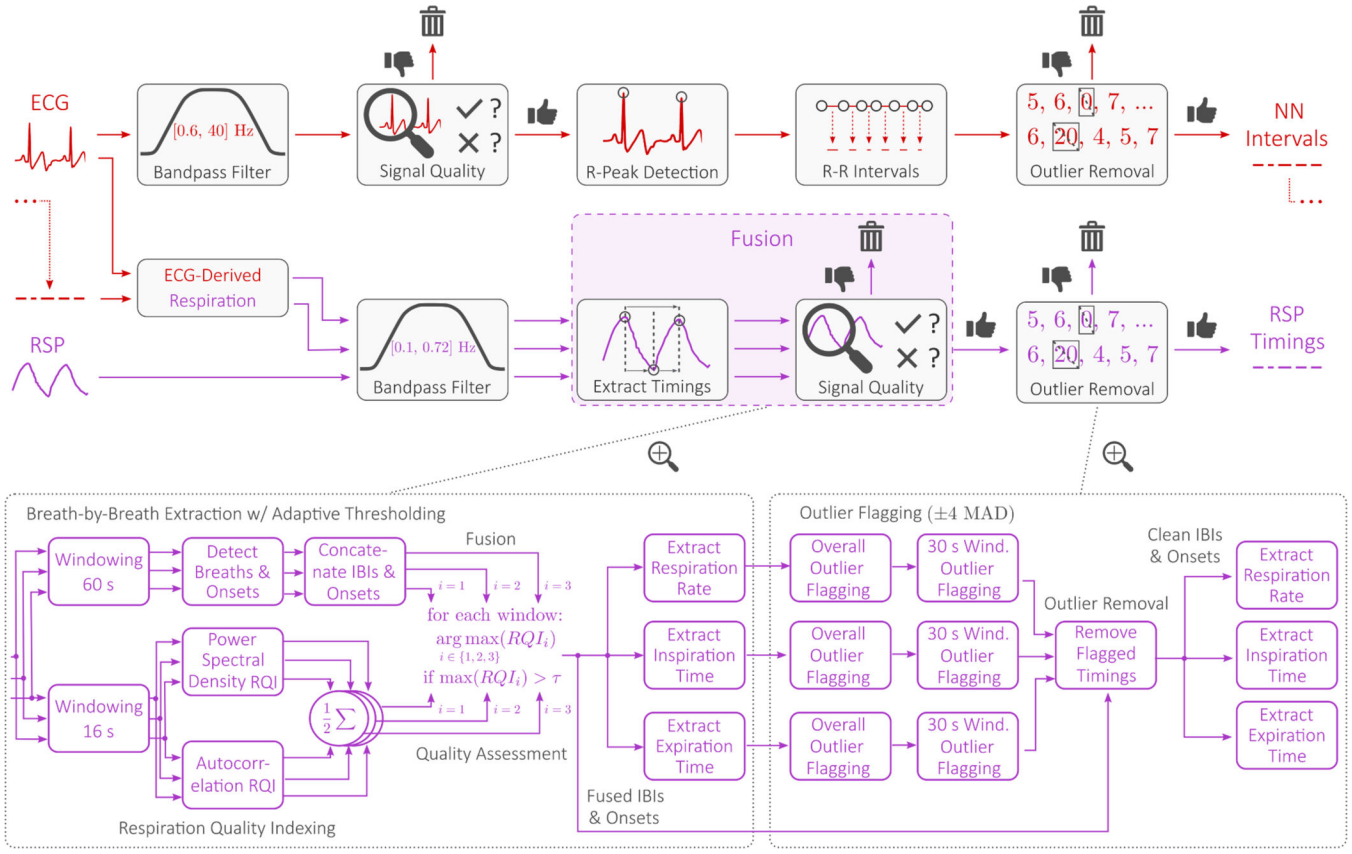

Fig. 3. Signal processing and respiration timing extraction block diagram.

The electrocardiogram (ECG) is first bandpass filtered and assessed for signal quality. R peaks are then detected, and R-R intervals are computed by finding the time differences; this is followed by outlier removal. These quality normal to normal (NN) intervals are then used along with the original ECG signal to estimate two ECG-derived respiration signals; these signals are considered along with the belt-based respiration signal also measured. All three signals are bandpass filtered and used as detailed in the figure to derive robust respiration timing estimates. The necessary low-level details are depicted beneath the feature-level fusion and quality assessment components.

Author Manuscript Author Manuscript Author Manuscript Author Manuscript

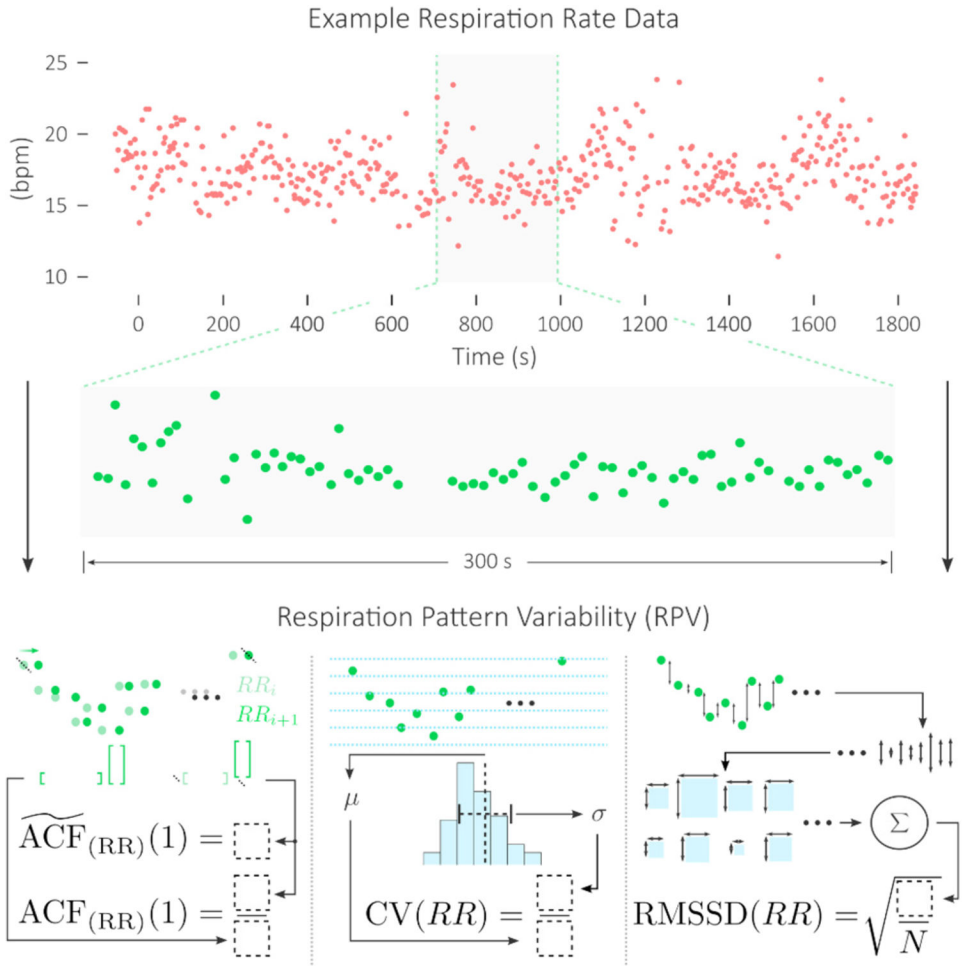

Fig. 4. Respiration pattern variability metrics investigated in this work.

Example data and illustrations of the respiration pattern variability (RPV) metrics investigated in this work. Respiration timings in time series form are windowed using a rolling window of 300 s with 299 s overlap to extract four RPV metrics. The first two are related to the autocorrelation exhibited by the window of data at one lag, unscaled and scaled. The third is the coefficient of variation (CV) and the fourth is the root mean square of successive differences (RMSSD).

Author Manuscript Author Manuscript Author Manuscript Author Manuscript

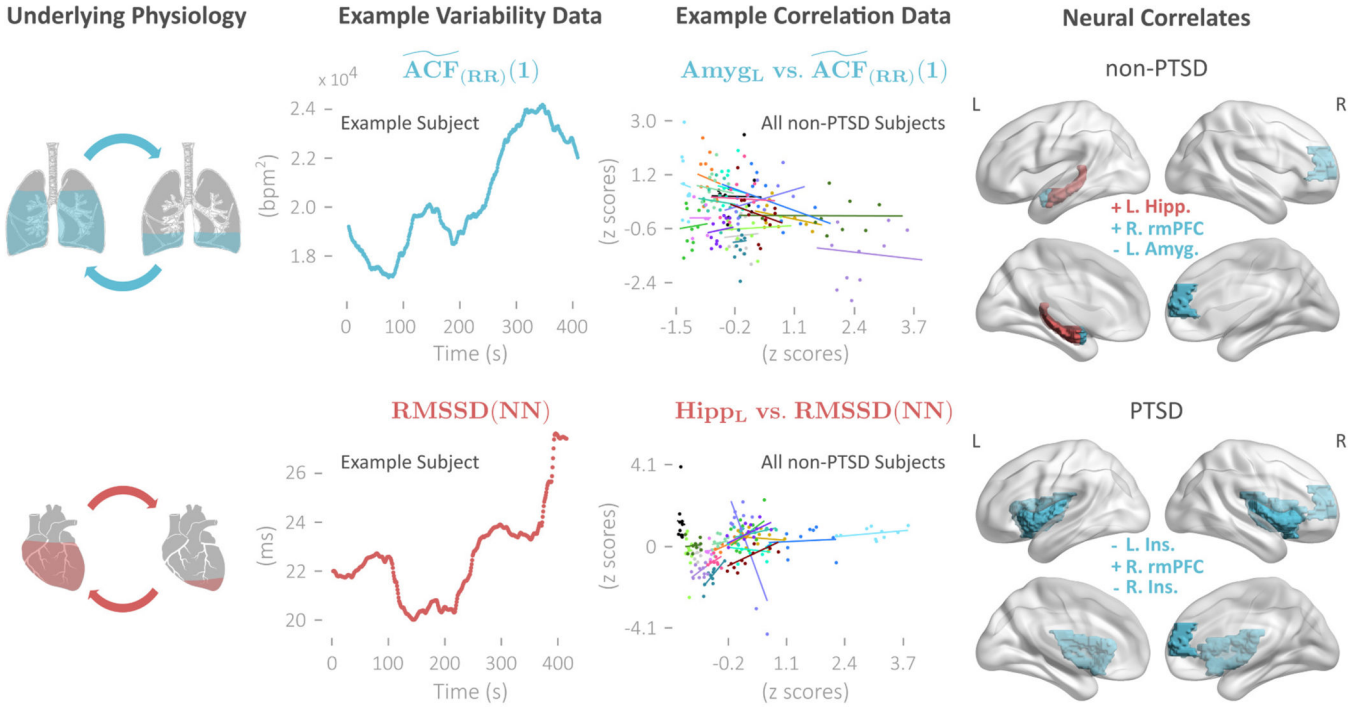

Fig. 5. Neural correlates of respiratory and heart rate variability for both PTSD and non-PTSD.

On the furthest left, the underlying physiological processes driving changes in cardiac and respiratory timings are simplistically illustrated; to the right of that, example variability features found pertinent to neuroactivity in key limbic regions are plotted for a single subject during approximately the same time window. Second from the right are two examples of statistically significant mixed modeling-based correlation plots illustrating the subject-specific slopes and intercepts used to fit the data, where subject ID is equivalently colored in the two plots shown (non-PTSD group). Furthest right are the neural correlates depicted in lateral views of 3-D renderings with the specific brain regions and correlation signs shown. Hipp. is short for hippocampus, amyg. Is short for amygdala, and rmPFC is the acronym for rostromedial prefrontal cortex; L. for left hemisphere and R. for right hemisphere. All correlations shown were statistically significant with $p < .05$ (corrected).

Author Manuscript Author Manuscript Author Manuscript Author Manuscript

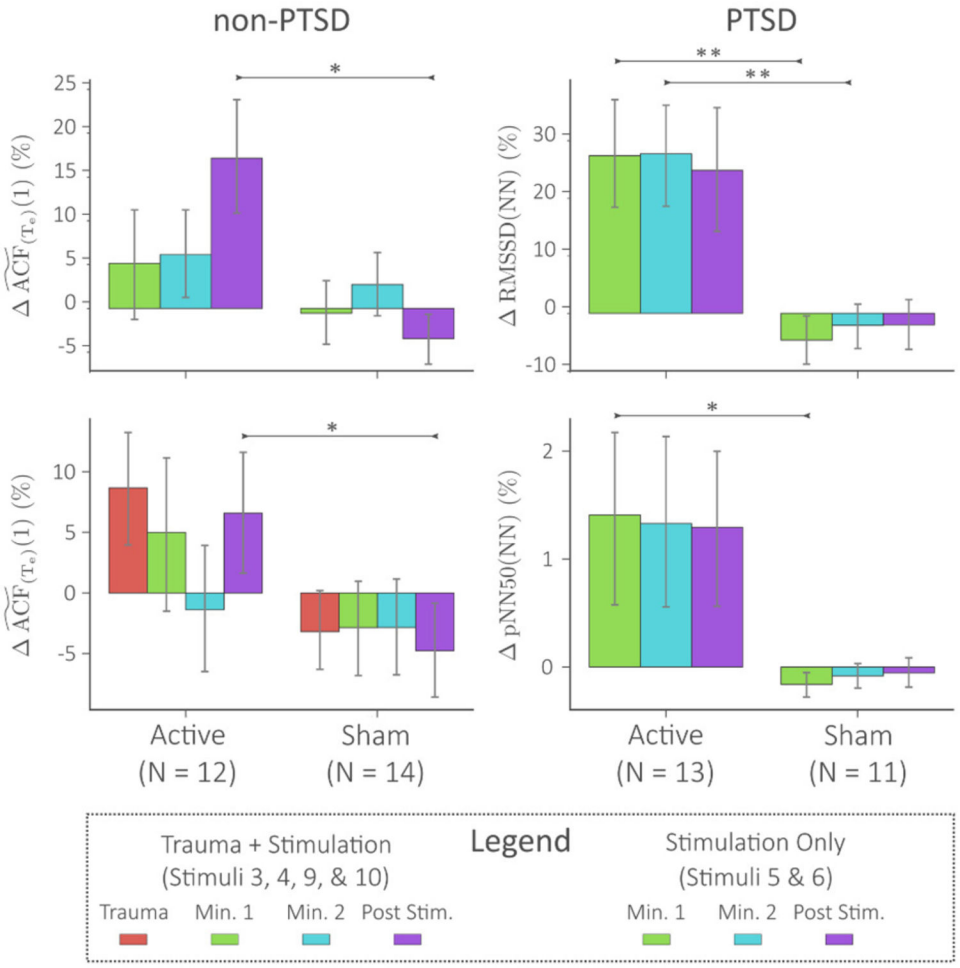

Fig. 6. Active tcVNS vs. sham stimulation comparison for both PTSD and non-PTSD.

The non-PTSD group is shown on the left, where the unscaled autocorrelation in expiration time significantly differed in the post-stimulation period between the active and sham groups. This was both for stimulation with no immediately preceding traumatic stress (top left) and stimulation immediately following traumatic stress (bottom left). For the PTSD group on the right, heart rate variability differences were found that were not previously investigated during stimulation with no immediately preceding stress. * denotes $p < .05$ (corrected), and ** denotes $p < .01$ (corrected). Data in bar plots represent mean ± SEM.